creative commons
COMMONS DEED

저작자표시-비영리-변경금지 2.0 대한민국

이용자는 아래의 조건을 따르는 경우에 한하여 자유롭게

- 이 저작물을 복제, 배포, 전송, 전시, 공연 및 방송할 수 있습니다.

다음과 같은 조건을 따라야 합니다:

저작자표시. 귀하는 원저작자를 표시하여야 합니다.

비영리. 귀하는 이 저작물을 영리 목적으로 이용할 수 없습니다.

변경금지. 귀하는 이 저작물을 개작, 변형 또는 가공할 수 없습니다.

- 귀하는, 이 저작물의 재이용이나 배포의 경우, 이 저작물에 적용된 이용허락조건을 명확하게 나타내어야 합니다.
- 저작권자로부터 별도의 허가를 받으면 이러한 조건들은 적용되지 않습니다.

저작권법에 따른 이용자의 권리는 위의 내용에 의하여 영향을 받지 않습니다.

이것은 이용허락규약(Legal Code)을 이해하기 쉽게 요약한 것입니다.

Disclaimer

dCollection

의학박사 학위논문

Rat에서 탄탈륨 이온이 코팅된 실리콘 보형물의 피막형성 감소효과

The reduced capsular formations on Tantalum-ion coated silicone implants in rats

2020년 2월

서울대학교 대학원
의학과 성형외과학전공
이 시 우

Abstract

The reduced capsular formations on Tantalum-ion coated silicone implants in rats

Siwoo Lee

Department of Plastic and Reconstructive Surgery

The Graduate School of College of Medicine

Seoul National University

Background: Although the design of more biocompatible polymeric implants has been studied for decades, their intended functionality continues to be impaired by the response of the host tissue to foreign bodies at the tissue–implant interface. In particular, the formation and contracture of fibrous capsules prevent the intimate integration of an implant with surrounding tissues, which leads to structural deformation of the implants and persistent discomfort and pain.

Methods: Silicone implants were coated with Ta-ion using a new technique called sputtering-based plasma immersion ion implantation (S-PIII). Surface characterisctics, wettability and mechanical properties were evaluated. The *in vitro* cellular responses of the bare and S-PIII treated silicone implants were evaluated via cell proliferation and viability with human dermal fibroblasts. In addition, an 8-week *in vivo* study was conducted. Bare and nano/Ta

silicone implants were inserted beneath the panniculus carnosus muscle of rats and foreign body responses at the tissue‐implant interface were comprehensively compared.

Results: S-PIII can introduce a biologically compatible tantalum (Ta) on the silicone surface to produce a Ta-implanted skin layer (<60nm thick) as well as generate either smooth (Smooth/Ta silicone) or nano-textured (Nano/Ta silicone) surface morphologies. The biologically inert chemical structure and strong hydrophobic surface characteristics of bare silicone are substantially ameliorated after Ta ion implantation.

Cell proliferation and viability of the nano/Ta silicone were improved in the *in vitro* study. In the *in vivo* study, the Nano/Ta silicone implant inhibited fibrous capsule formation and contracture on its surface better than the bare silicone based on an analysis of the number of macrophages, myofibroblast differentiation and activation, collagen density, and thickness of fibrous capsules.

Conclusion: Capsular formations were reduced on Tantalum-ion coated silicone implants in rats

---

keywords : Silicone, tantalum, ion implantation, foreign body response

***Student Number* : 2014-30650**

CONTENTS

LIST OF FIGURES

LIST OF TABLES

I. Introduction

Advances in medical technology and an increased life expectancy have contributed to the rapidly increasing demand for reliable and efficient medical implants to improve the quality of human life [1, 2]. Many versatile polymeric materials have been employed and adapted for implant fabrication according to their physical and chemical attributes [3]. However, these polymers often induce a foreign body response at the tissue–device interface, which includes inflammation, fibrosis, thrombosis, and infection. This may persist for the entire lifetime of an implant and adversely affect its intended functionality [4, 5]. In particular, the formation of a thick and dense fibrous capsule (i.e., a specific feature consisting of large numbers of neutrophils, macrophages, and leukocytes) around an implant may block intimate interactions between the host tissue and implant surface; this can eventually lead to structural deformation of the implant, reduced efficiency, and eventual failure [1, 4, 6, 7]. In addition, capsular voids easily occur; this increases bacterial infection and invasion, which induces acute and chronic inflammation reactions [8]. Furthermore, recent studies on breast implant-associated anaplastic large cell lymphoma (BIA-ALCL) have increased the need for new types of silicone implants. As BIA-ALCL is mainly generated in texture-type silicone implants, discussions on microtexture- or smooth-type implants have been revived.

For decades, many researchers have explored reducing the foreign body response associated with polymeric devices by modifying material surfaces to

directly incorporate biological factors such as antibiotics, enzymes, proteins, and drugs [4, 9-11]. However, their poor adhesion stability to the substrate and unacceptable mechanical properties have been a major drawback and directly associated with potential safety issues for some applications. For example, an immobilized anti-inflammatory agent on the implant surface can induce a burst release of a lethal dose under physiologically harsh conditions, which can trigger undesirable side effects in the host tissue [12]. Furthermore, many of these agents retard angiogenesis, which can readily result in poor blood circulation around the implant [4].

Over the past few decades, it has become evident that the surface topography plays a critical role in obtaining a favorable biological response to a material that results in intimate interfacial contact with adjacent tissues [13-15]. In particular, nano-textured surfaces where surface structures have dimensions of less than 100nm possess unique properties compared to smooth surfaces because of their similar structural dimensions to those of the natural extracellular matrix and large surface area relative to their volume. These properties are highly beneficial for promoting early mammalian cell adhesion/proliferation and suppressing inflammatory responses [13, 16]. After implantation, rapid cell adhesion, spreading, and proliferation not only promote adhesion to the surrounding tissue and close contact formation but also reduce the chance of neutrophils or monocytes to adhere to the implant [17]. Consequently, mechanically stable and biologically intimate integration is attained at the implant–tissue interface, which reduces the width between the implant and host tissue as well as fibrotic tissue formation [18].

Owing to these tremendous biological benefits, many studies have been conducted on the development of nano-textured surfaces on polymeric substrates [19, 20]. Currently, surface nanoimprinting is the most widely used nanofabrication technique, where the polymer surface is physically deformed into steps through the use of a pre-patterned rigid mold under pressure [21]. The ability to replicate biologically relevant patterns on the polymer substrate at the nanometer scale and the simplicity of the process make nanoimprinting an attractive fabrication technique for biomedical applications. However, despite its many advantages, it is not compatible with curved and nonplanar surfaces because of the difficulty in completely covering the substrate surface [22]. This limitation on the narrow set of applicable substrate features has drastically reduced the potential impact of this technique on 3D complex-shaped medical implants.

Recently, plasma immersion ion implantation (PIII) has been introduced as a promising surface modification strategy because of its non-line-of-sight characteristic, which is beneficial for the treatment of complex-shaped implants [23]. During PIII treatment, a bias voltage is applied to generate an ion sheath that follows the surface profile of an irregularly shaped implant, and gaseous plasma ions are homogeneously irradiated over the entire surface. This energetic ion injection can disrupt the surface structure of an implant by displacement or removal of the surface atoms, which results in a relatively rough surface morphology [24]. However, despite its obvious advantages, most reports on PIII treatment to date have shown poorly developed surface nano-textures with a roughness of no more than a few nanometers [25-27]. Commonly used gaseous ion implantation sources such as

oxygen, nitrogen, and argon may not be suitable for the development of distinct surface nano-textures with a sufficient depth (i.e. up to 100nm) because their mass is innately very light.

In the continuous effort to develop an efficient method of fabricating well-defined nano-textured surfaces, a sputtering-based PIII (S-PIII) technique was developed for the first time that uses a DC magnetron sputtering target gun to introduce tantalum (Ta), which is one of the heaviest elements among biocompatible materials, as a plasma ion source. During the S-PIII treatment, numerous Ta ions are emitted from the Ta target surface; subsequently, the implant is subjected to a markedly high dose and rate ion implantation as a high negative bias voltage is applied. This is sufficient to rigorously etch the implant and generate distinct nanostructures on its surface. In this study, silicone was chosen as a representative polymeric substrate because it has been extensively utilized in the production of artificial biomedical devices but suffers from insufficient biocompatibility and a high occurrence rate of foreign body response [28, 29]. Ta ions were directly implanted onto the commercial silicone implants with the S-PIII technique, and the surface characteristics of the modified silicone were evaluated in terms of the morphology, roughness, chemical composition, and wettability. The synergistic effect of the nano-textured surface as a physical cue and the implanted Ta element as a chemical cue was investigated through *in vitro* and *in vivo* experiments.

II. Material and Methods

2.1. Sample preparation

Commercial silicone implants (SOFTXIL, Bistool, Korea) with dimensions of 10mm × 10mm × 1mm were prepared for the surface characterization, adhesion stability test, contact angle measurement, and *in vitro* cellular response evaluation. All samples were cleaned ultrasonically in alcohol and deionized water for 5 min before the S-PIII process. A Ta target (75mm diameter, 5mm thickness, 99.99% purity, Kojundo Chemical Lab, Japan) was placed in a DC magnetron sputtering gun (Ultech Co. Ltd., Daegu, Korea), and the vacuum chamber was initially pumped to 5×10^{-4} Pa with rotary and diffusion pumps. To generate sufficient amounts of Ta ions and neutral atoms, 12W of target power was applied to the Ta sputtering gun, and the working pressure and temperature were maintained at 0.6 Pa and 25°C, respectively, during the process. The silicone implants were placed on a metal back-plate parallel to the Ta target surface at a distance of 60mm. A high negative substrate voltage bias (−2000V) was applied to the metal back-plate. The treated silicone implants were designated as Nano/Ta silicone. In addition, untreated silicone implants (bare silicone) were used as the control group. For the *in vivo* experiments, elliptically shaped silicone rubber samples with dimensions of 15mm (diameter) × 5mm (height) were prepared, and S-PIII was conducted on the whole surface as it was rotated. Other processing conditions were kept the same.

2.2. Surface characterization and Ta ion release

The surface morphology was observed by field-emission scanning electron microscopy (FE-SEM; JSM-6330F, JEOL, Japan). The surface roughness (R_a) was calculated with atomic force microscopy (AFM; NANO Station II, Surface Imaging Systems, Germany). The surface chemical compositions and elemental depth profiles were determined by X-ray photoelectron spectroscopy (XPS; AXIS-HSi; Shimadzu/Kratos, Kyoto, Japan) with a monochromatic Al K_α source. The Ta depth profiles were acquired by XPS in conjunction with argon ion bombardment at a sputtering rate of about 4nm/min.

Two types of Ta-implanted silicone implants were immersed in 10mL of phosphate buffered saline (PBS, pH 7.4) for 7, 14, 21, and 28 days at 37°C without stirring. At each prescribed time, the entire 10mL solution was taken and analyzed with an inductively-coupled plasma mass spectrometer (ICP-MS, NexION 350D, Perkin-Elmer, USA) to determine the amount of released Ta. The withdrawn solution was replaced with the same volume of fresh phosphate-buffered saline (PBS, pH 7.4; WELGENE Inc., Korea). To investigate the changes in the structure morphology and surface chemical composition, FE-SEM, AFM, and energy-dispersive X-ray spectroscopy (EDS) elemental mapping analysis were performed on the implants after immersion in PBS for 28 days.

2.3. Wettability and Mechanical property evaluation

The hydrophilicity of the silicone implants, which is known to correlate closely with cell behavior, was evaluated with the sessile drop method. A distilled water droplet was placed onto each silicone implant surface and photographed with a charge-coupled device (CCD) camera connected to a goniometer (Phoenix 300, Surface Electro Optics Co. Ltd., Korea). The contact angle between the distilled water drop and surface was calculated with image analysis software (Image XP, Surface Electro Optics Co. Ltd., Korea).

To investigate the effect of 120s of Ta S-PIII treatment on the intrinsic mechanical properties of a silicone implant, a tensile test was conducted with a universal testing machine (Instron 5543, Instron Corp., Canton, MA) at a fixed loading rate of 50mm/min until rupture. A rectangular piece of silicone implant with a length of 40 mm and width of 10 mm was used. The maximum stress was measured and converted to the tensile strength (MPa). At least four of each kind of sample were measured.

2.4. *in vitro* cell viability

The *in vitro* cellular responses of the bare and S-PIII treated silicone implants were evaluated via cell proliferation and viability with human dermal fibroblasts, as described in previous studies [4, 30, 31]. Pre-incubated cells were seeded onto the specimens at a density of cells/mL for the

cell-proliferation assay and cell viability. After culturing fibroblast for 5 days, cell proliferation was examined through a cell counting kit-8 (CCK-8, Dojindo, Rockville, MD) assay and a methoxyphenyl tetrazolium salt (MTS, Promega, Madison, WI) assay with calculating 450nm and 490nm absorbance repectively (A_{450}, A_{490}). In addition, the cell viability rate was calculated by dividing cell proliferation of samples by cell proliferation of TCP(tissue culturing plate).

2.5. *in vivo* animal experiments

For the *in vivo* animal experiments, 8-week-old Sprague-Dawley rats weighing 250g were used. The animals were maintained in a temperature-controlled room (22°C) on a 12 h:12 h light–dark cycle under specific-pathogen-free (SPF) conditions with free access to food and water. All procedures were approved by the Institutional Animal Care and Use Committee (IACUC) of Seoul National University Hospital (IACUC No. 2018-0007). In this test, the animals were divided into two groups according to the implant sample inserted: bare silicone and Nano/Ta silicone implants. Each experiment group comprised seven animals for evaluation.

For the implant insertion, all surgical procedures were performed under aseptic conditions by the same individual (J.U.P.). The surgical field was prepared with 10% povidone-iodine, and a single dose of cefazolin (60 mg kg^{-1}) was administered intramuscularly for the prophylaxis of infection. The animals were anesthetized with an intraperitoneal injection of Zoletil (30 mg

kg^{-1}) and Rumpun (5mg kg^{-1}). Smooth-surfaced silicone implants were used that are solid hemispheres with a diameter of 15 mm, which were sterilized by autoclaving and exposure to ultraviolet light (**Fig. 1A**).

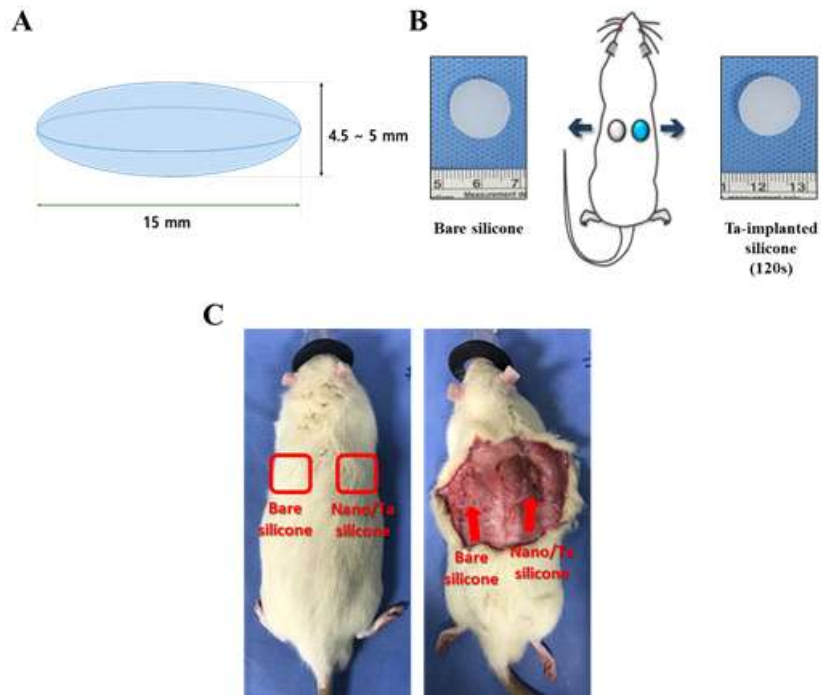

Fig. 1. (A) Schematic illustration of the silicone implant and its dimensions used in the *in vivo* animal test. (B) *In vivo* rat dorsal implantation model. (C) Optical views of the implanted bare and Nano/Ta silicone samples after 8 weeks of surgery.

Two subcutaneous pockets for implant insertion were made on the back of each rat through two separate 2-cm-long vertical incisions that were started at a lateral position 1.5 cm to the side of the midline and 1cm below the shoulder bone (**Figs. 1B and C**). The implants were inserted beneath the panniculus carnosus muscle. The surgical wounds were closed with successive layers of 4-0 Vicryl and 5-0 Ethilon (Ethicon, Inc., USA).

After 8 weeks, the rats were sacrificed by CO_2 asphyxiation in accordance with the American Veterinary Medical Association (AVMA) Guidelines for the Euthanasia of Animals. The fibrous capsular tissue formed surrounding the silicone implants was retrieved through a skin incision.

The fibrous capsule tissues were fixed overnight in 4% paraformaldehyde (PFA), embedded in paraffin, and cut into 4-μm sections for hematoxylin and eosin (H&E) staining. Each stained slide was examined at 100× magnification with a Leica DM2500 microscope (Leica MicrosystemsSwitzerland, Ltd, Switzerland), and images were captured from three microscopic fields: right, center, and left. The capsular thickness was measured at the maximal point with Image J 1.36b imaging software (National Institutes of Health, Bethesda, MD, USA). The collagen density around the implant was evaluated with Masson's trichrome (MT) staining. The area of the blue-stained collagen was measured from the sample image observed at 100× magnification with Image J software. The selected area was then calibrated to give the percentile value based on the whole area of the tissue in the same image. To count the numbers of cells such as macrophages, fibroblasts, and myofibroblasts, immunohistochemistry (IHC) staining was performed with the primary anti-CD68, anti-vimentin, and anti-αSMA. The fibrosis-related cells (i.e., macrophages, fibroblasts, and myofibroblast) were manually counted in the unit area captured from the three microscopic fields (right, center, and left).

Capsular tissues were solubilized by sonication in a radioimmunoprecipitation assay buffer containing protease inhibitors (Pierce, Rockford, IL), and the protein concentration was measured with a BCA

protein assay kit (Thermo-Fisher, Seoul, Republic of Korea). After being denatured by boiling, the protein sample (20 μg for each lane) was separated by 10% sodium dodecyl sulfate-polyacrylamide gel electrophoresis and transferred to a polyvinylidene fluoride (PVDF) membrane (Millipore, Boston, MA). The blot was probed with a primary antibody [rabbit polyclonal to connective tissue growth factor (CTGF, C Terminus, IHCplus6) (1 : 100)], rabbit αSMA antibody (1 : 1,000), rabbit vimentin antibody (1 : 1,000), rat COL I antibody (1 : 1,000), rat monoclonal to transforming growth factor β (TGF-β, 1 : 50), goat myeloperoxidase (MPO) antibody (1 : 1,000), rabbit polyclonal vascular endothelial growth factor (VEGF, 1 : 1,000), or rat monoclonal β-actin, (1 : 1,000)] in a blocking solution of 5% BSA in TBST overnight at 4 °C and then incubated with peroxidase-conjugated secondary antibodies (1:5000) for 1 h at room temperature. The immunolabeled proteins were detected by chemiluminescence with a SuperSignal ECL kit (Pierce Chemical, Rockford, Ill) and ImageQuant LAS 4000 (GE Healthcare Life Science, Marlborough, MA, USA).

2.6. Statistical analysis

All assays were performed a minimum of n = 3 times per group. Statistical Package for the Social Sciences (SPSS 23, SPSS Inc., USA) was used for the statistical analysis. All numerical data were reported as mean ± standard deviations. The normality of the variables was tested with the

Shapiro–Wilk test, and the statistical analysis was performed by one-way analysis of variance (ANOVA) with Tukey post-hoc comparison. A p value below 0.05 was considered significant in all cases.

III. Results

3.1. Surface characterization

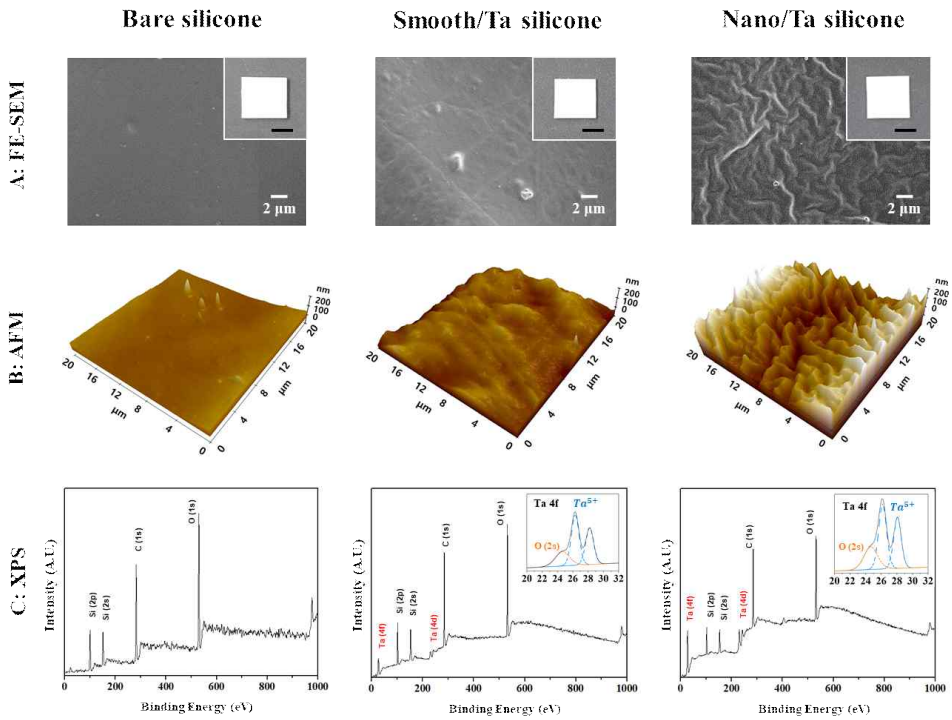

Fig. 2. Representative (A) FE-SEM images, (B) AFM topographical 3D maps, and (C) XPS full spectra obtained from bare, Smooth/Ta, and Nano/Ta silicone. The insets in the FE-SEM images and XPS results are macroscopic optical images and high-resolution spectra of Ta 4f for each silicone implant. Black scale bars indicate 5 mm.

The surface morphologies of the silicone implants before and after Ta ion implantation with different processing times (30s for Smooth/Ta silicone and

120s for Nano/Ta silicone) were investigated with a macroscopic optical view, FE-SEM, and AFM (**Figs. 2A** and **B**). The macroscopic images of each sample showed no apparent visible change on the silicone after Ta ion implantation up to 120s; all silicone samples preserved their rectangular shapes and whitish surfaces without the generation of defects or morphological irregularities. In contrast, the FE-SEM and AFM images showed that the surfaces of each Ta-implanted silicone implant were significantly different. Rough and wrinkled nanoscale structures were clearly present on the surface of the Nano/Ta silicone implant, whereas there was no significant topographical change on the surface of the Smooth/Ta silicone implant compared with the bare implant. The average surface roughness of the Nano/Ta silicone implant (R_a = 67 ± 6nm) was about 3.9 and 3.2 times higher than those of the bare (R_a = 17 ± 4nm) and the Smooth/Ta silicone (R_a = 21 ± 7nm) implants, respectively (**Table 1a**).

Table 1a. Mean- and maximum-height surface roughnesses (R_a and R_z) for the three types of silicone implants.

Surface roughness	**Bare silicone**	**Smooth/Ta silicone**	**Nano/Ta silicone**
R_a (nm)	17 ± 4	21 ± 7	67 ± 6
R_z (nm)	87 ± 16	91 ± 23	368 ± 34

XPS was applied to investigate the surface chemistry of all samples, and the results are shown in **Fig. 2C**. In the wide spectra, the bare silicone only exhibited its representative peaks (C 1s, O 1s, Si 2s, and 2p), whereas both Ta-implanted silicone samples showed additional metallic Ta peaks (Ta 4f

and 4d). The inserts in the figure show high-resolution spectra of Ta 4f and clearly present two distinctive peaks of Ta^{5+} at binding energies of 26.2 and 28.3 eV, which correspond to the typical Ta chemical state in Ta_2O_5 [32].

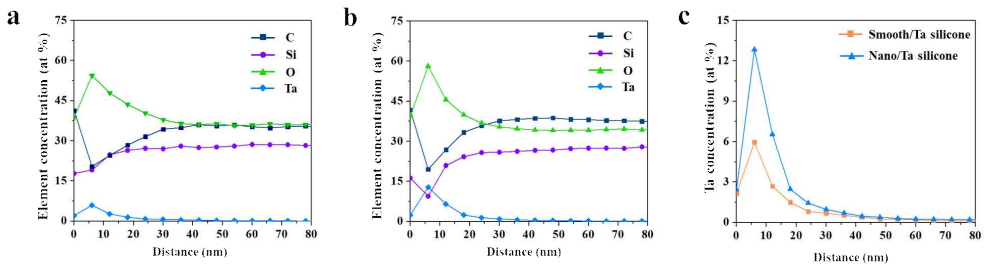

Fig. 3. XPS depth profile of the (a) Smooth/Ta and (b) Nano/Ta silicone implants; (c) relative concentrations of Ta as a function of depth for each silicone.

XPS depth profiling was performed for further quantitative analysis of the surface elements and their cross-sectional distributions (**Fig. 3**). Both the Smooth/Ta and Nano/Ta silicone implants showed almost identical Ta and O amounts on their uppermost surfaces. As the depth increased near the surface, their concentrations rapidly increased and then decreased with the highest concentration at a depth of 6nm. In contrast, C and Si showed the opposite tendency (**Figs. 3a** and **b**). The maximum levels of implanted Ta in the silicone surfaces were 5.9% and 12.8% for the Smooth/Ta and Nano/Ta silicone, respectively (**Fig. 3c**).

3.2. Surface stability and wettability

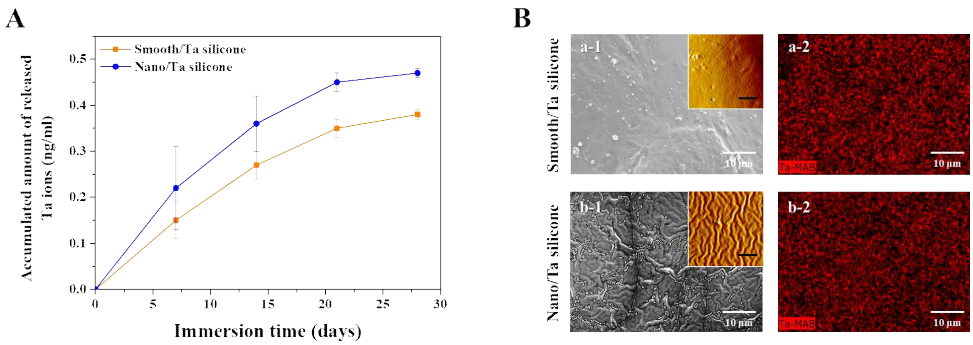

Fig. 4. (A) Accumulated amounts of released Ta ions from the surfaces of Smooth/Ta and Nano/Ta silicone. (B) Surface morphological and chemical changes of each silicone surface after 28 days of immersion: (a-1 and b-1) FE-SEM images and (a-2 and b-2) EDS mapping results (red color represents the Ta element). Black scale bars indicate 5μm.

In order to evaluate the surface stability of the Ta-implanted silicone surfaces under physiological conditions, the Smooth/Ta and Nano/Ta silicone implants were immersed in PBS at 37°C, and the amounts of released Ta ions were measured for up to 4 weeks. As shown in **Fig. 4A**, both silicone implants showed extremely low levels of released Ta ions from the implanted surfaces; Ta ions were slowly released into the medium without a significant initial burst for 1 week, and then their amount steadily decreased with the immersion time. In both cases, the release profiles of the Ta ions reached nearly saturation levels after about 4 weeks of immersion.

After the immersion test, the surface morphological changes and remaining Ta element on the silicone surface were further investigated by FE-SEM, AFM, and EDS mapping analysis (**Fig. 4B**). Tiny precipitated particles were

formed and randomly distributed on both Ta-implanted silicone surfaces, but each surface preserved their initial surface morphologies without any noticeable differences before and after the immersion testing (**Figs. 4Ba-1** and **b-1**). The AFM results consistently showed no significant changes in the average surface roughness values, which were 25 ± 8 nm and 65 ± 7 nm for the Smooth/Ta and Nano/Ta silicone, respectively (**Table 1b**).

Table 1b. Mean- and maximum-height surface roughnesses (R_a and R_z) of Smooth/Ta and Nano/Ta silicone after 28 days of immersion in PBS.

Surface roughness	**Smooth/Ta silicone**	**Nano/Ta silicone**
R_a (nm)	25 ± 8	65 ± 7
R_z (nm)	144 ± 5	404 ± 35

The EDS mapping and analysis data clearly showed that the remaining Ta had a uniform distribution over the whole surface of both the Smooth/Ta and Nano/Ta silicone implants (**Figs. 4Ba-2** and **b-2**).

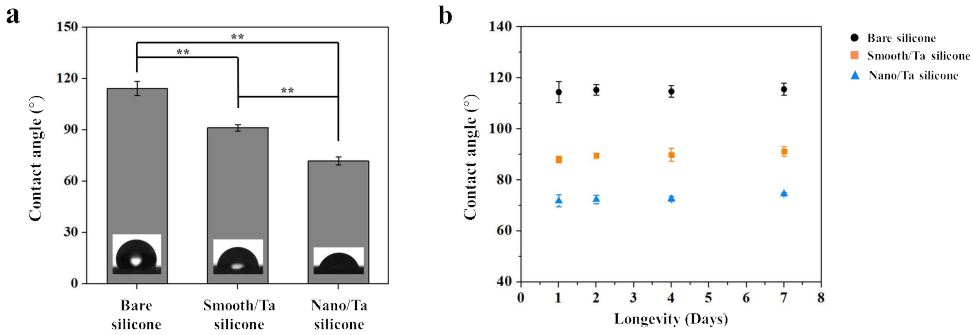

Fig. 5. (a) Contact angles of bare, Smooth/Ta, and Nano/Ta silicone implants and (b) their longevity as a function of time. Representative optical images of sessile droplets on each silicone surface are shown as insets. The statistical significance is indicated by **$p < 0.01$.

The wettability of each silicone implant was measured from the static water contact angle, as shown in **Fig. 5a**. The bare silicone surface exhibited typical hydrophobicity with a contact angle of 110°, which matched the results from previous studies well [33]. In contrast, both silicone surfaces after Ta ion implantation had significantly improved hydrophilicity with contact angles of less than 90°. In particular, the Nano/Ta silicone exhibited the lowest contact angle of around 75° among the three silicone implant groups; this remained almost unchanged for 7 days, which indicates long-lasting surface hydrophilicity (**Fig. 5b**).

3.3. Mechanical properties of Ta-implanted silicone

To investigate the effect of the Ta ion implantation on the deterioration of the mechanical properties of the silicone implants, the tensile properties

of the Nano/Ta silicone implant (i.e., the sample with the longest S-PIII treatment) were tested and compared with those of the bare silicone. As shown in **Fig. 6a**, the stress–strain curves of both silicone implants were similar in shape, although the tensile strength of the Nano/Ta silicone was slightly higher than that of the bare one (3.7 ± 0.1 MPa for bare silicone, 3.8 ± 0.2 MPa for Nano/Ta silicone). However, this was not significant ($p > 0.05$) (**Fig. 6b**). A similar tendency was observed in the strain at failure; the bare and Nano/Ta silicone implants showed strain at failure rates of 9.5 ± 0.2% and 9.2 ± 0.2%, respectively, and the difference between two implants was only 3.3% and not significant ($p > 0.05$) (**Fig. 6c**).

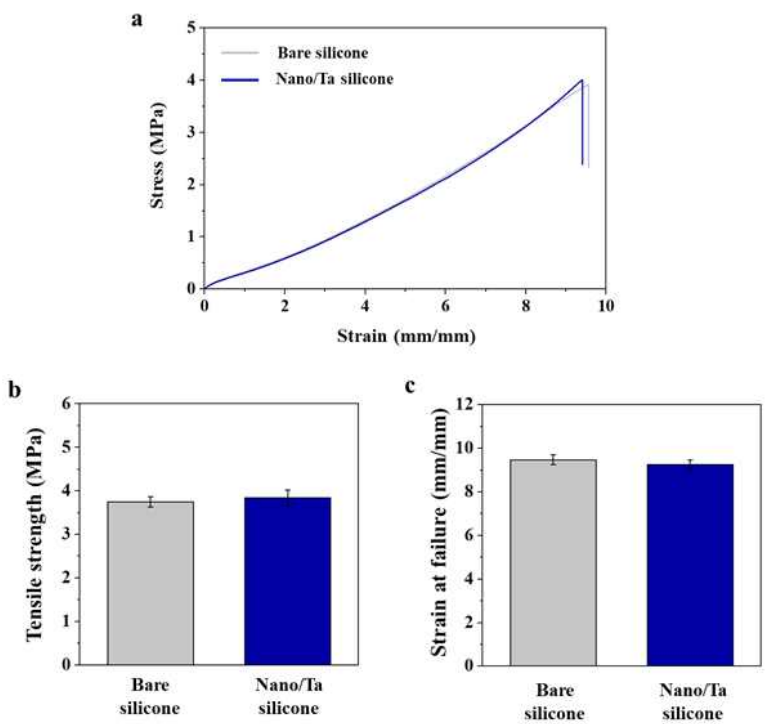

Fig. 6. (a) Stress–strain curve, (b) tensile strength, and (c) strain at failure of bare and Nano/Ta silicone implants

3.4. *in vitro* cell viability

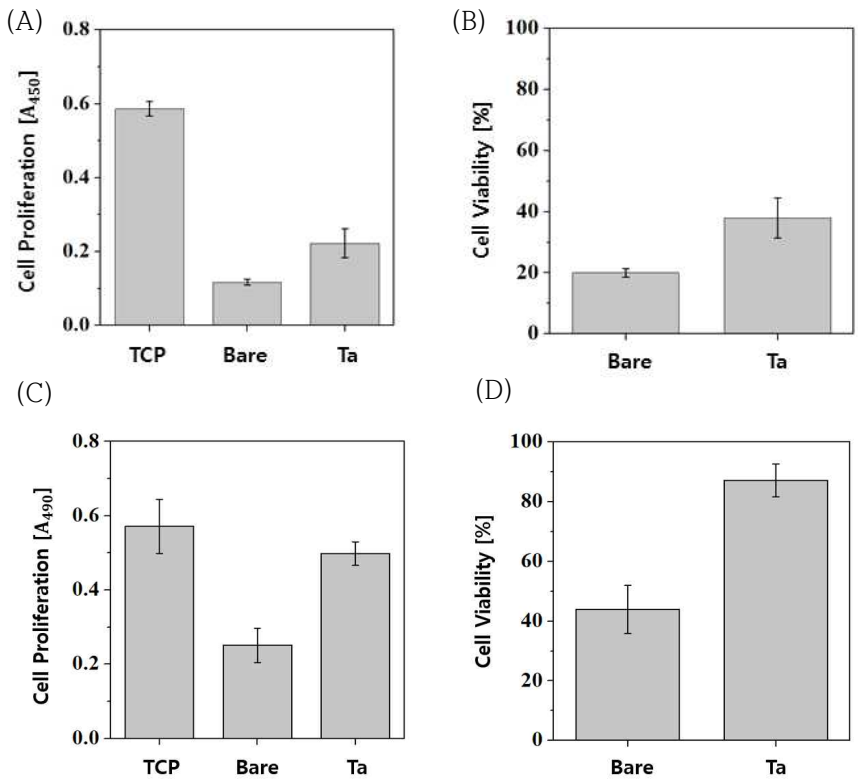

Fig. 7. (A) CCK-8 assay result of cell proliferation value of absorbance(450nm) of adhered fibroblasts cultured for 5 days on bare and Nano/Ta silicone implants. (B) CCK-8 assay result of cell viability rate. (C) MTS assay result of cell proliferation. (D) MTS assay result of cell viability. The statistical significance is indicated by $p < 0.05$

To assess the short-term tissue‐implant interface response, the response of human dermal fibroblasts to the implants in terms of cell viability and proliferation was closely examined. In **Figs. 7A and 7C,** even though the cells were cultured at the same concentrations, the values of absorbance

were different according to the difference of CCK-8 and MTS assay. **Fig. 7A** shows that in the CCK-8 value, the absorbance of TCP is high while the absorbance of the sample is low. Accordingly, the cell viability value, which is the proliferation value of each sample divided to TCP, is calculated lower than in MTS value. But, the difference between bare and tantalum surfaced samples is clearly visible in both the CCK-8 and MTS assay (**Fig. 7B, 7D**)

3.5. In vivo foreign body response

3.5.1. Histological analysis of fibrous capsules

To evaluate whether the S-PIII treatment can suppress the foreign body response, Nano/Ta silicone implants, which showed better cellular responses in the *in vitro* study, were inserted into the interstitial connective tissue beneath the panniculus carnosus muscle layer in the dorsal skin of rats (**Fig. 1**). The bare silicone implants were tested as a control to represent the current clinical standard. After 8 weeks of implantation, the accumulated extracellular matrix (ECM) and cells around the implants were histologically analyzed, as shown in **Fig. 8**. The H&E stained images showed that the Nano/Ta silicone had significantly reduced ECM accumulation and capsule formation around the implant compared to the bare sample with capsular thicknesses of 203.6 ± 10.9 μm and 349 ± 45.9 μm, respectively. The bare silicone implant showed a thick fibrous capsule rich in cells with several

round clear cytoplasmic vacuoles that appeared uniformly throughout, whereas the Nano/Ta silicone only showed a few scattered cells mainly in close contact with the implant surface. The density of the collagen in the capsular tissue, which is a major ECM component of the fibrous capsule [4, 34], was morphometrically analyzed by MT staining. Collagen fiber bundles were more densely but irregularly accumulated on the bare silicone compared to on the Nano/Ta silicone; the latter showed highly porous interconnected networks of fibers with a parallel arrangement to the implant surface. The collagen density increased significantly in the bare silicone compared to the Nano/Ta silicone at 8 weeks ($p < 0.05$).

Immunohistochemical staining was carried out to investigate the expressions of fibroblast (vimentin), myofibroblast (αSMA), and macrophage (CD68) markers in the tissue; these are closely related to capsule formation and contracture [2, 6, 35]. Fibroblasts formed irregular clusters of separately aggregated cells and showed significant growth with high density in the capsule on the bare silicone; in contrast, they were virtually absent from tissue forming on the Nano/Ta silicone implant. In addition, multiple layers of densely packed myofibroblasts was only observed for the bare silicone implant, and the density was almost 2.5 times higher than that for the Nano/Ta silicone. The macrophage analysis also consistently showed similar foreign body responses; the Nano/Ta silicone implant had significantly fewer CD68-positive macrophages than the bare implant (bare silicone: 35.7 ± 2.6; Nano/Ta silicone: 25.3 ± 0.7; $p < 0.05$).

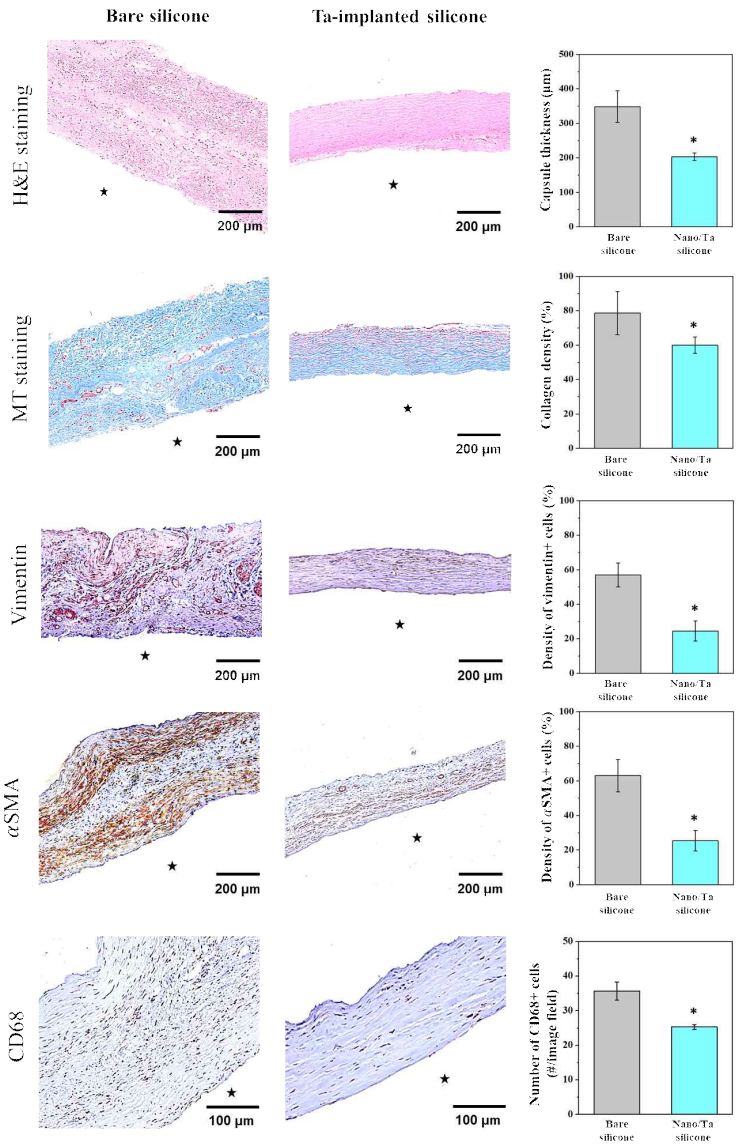

Fig. 8. Representative histological images of fibrous capsules formed around bare and Nano/Ta silicone implants stained with H&E and MT; the capsule and collagen-rich ECM are stained as red and blue, respectively. Fibroblasts, myofibroblasts, and macrophage accumulations are visualized by immunohistochemical staining of vimentin, αSMA, and CD68, respectively. The capsule thickness, density of collagen, fibroblasts, and myofibroblasts, and number of macrophages are quantified by image analysis. The statistical significance is indicated by *$p < 0.05$. Star symbols (★) indicate sites of silicone implantation.

3.5.2. Western blot analysis

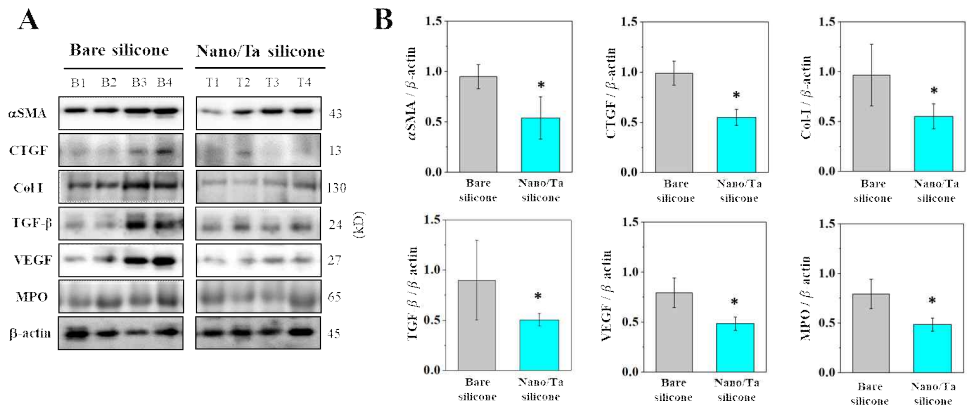

Fig. 9. (A) Representative Western blots and (B) expression levels of αSMA, CTGF, Col I, TGF-β, VEGF, and MPO in developed fibrous capsules around bare and Nano/Ta silicone implants. The relative levels are normalized to the housekeeping gene (β-actin). The statistical significance is indicated by *p < 0.05.

For a closer look at the factors closely related to capsule formation after silicone implant insertion in the tissue, western blot analysis was performed on the protein expressions of αSMA, CTGF, Col I, TGF-β, VEGF, and MPO. The levels of αSMA, CTGF, Col I, and TGF-β have positive correlations with myofibroblast differentiation and fibrosis progression, and VEGF and MPO reflect the degrees of platelet and neutrophil activation, respectively [35]. As shown in **Figs. 9A** and **B**, all protein expressions in the Nano/Ta silicone implant were substantially down regulated with weaker western blotting images and lower quantitative scores than the bare implant that were statistically significant ($p < 0.05$). In particular, α-SMA and Col I expressions greatly decreased by around 50% with the Nano/Ta silicone

compared to the bare silicone, which is consistent with the histological examination results shown in **Fig. 8**.

IV. Discussion

In this study, it is confirmed that the fibrous capsule formation around silicone implants can be substantially suppressed by the introduction of a nano-textured surface topography and Ta-implanted surface chemistry. Because Ta is known to have excellent biocompatibility and safety, this modification to the surface topography and chemistry may reduce the foreign body response at the tissue–implant interface and induce biologically intimate integration with the host tissue [36-38]. Furthermore, the proposed surface modification technique can be directly applied to commercial implants with complex 3D geometry.

The silicone implant surface was modified with the S-PIII method, in which a high dose of Ta ions generated from the sputtering target gun is implanted into the uppermost surface of a 3D complex shaped substrate while a negative substrate bias is applied. The large amount of implanted ions not only ensures an extremely short processing time but also minimizes the deterioration of the mechanical properties of the silicone implant (**Fig. 6**). Furthermore, the topography of the Ta-implanted silicone surface can be modified by changing the processing time; the bare, Smooth/Ta, and Nano/Ta silicone implants were compared to understand the effects of the surface topography and chemistry on the silicone surface properties. With a short processing time (30s), the silicone surface underwent energetic ion irradiation and implantation, and a relatively smooth but Ta-implanted stiff silicone skin layer was formed by the volumetric compaction and material

densification induced by the energetic collision cascade of the incoming Ta ions [39]. The cross-sectional XPS elemental analysis clearly indicated the existence of a Ta-implanted surface skin layer with a thickness of less than 60nm on the silicone implant (**Fig. 3**). At a longer processing time (120s), more Ta was implanted into the silicone surface; this severely compressed the outer surface, and the in-plane compressive stress was sufficiently increased to induce an out-of-plane deformation of the surface layer because of a mechanical property mismatch [40]. This caused a nano-textured surface and significant changes to the surface roughness (**Figs. 2A** and **B**).

As shown in **Fig. 2C**, both silicone implants with S-PIII treatment (i.e., Smooth/Ta silicone and Nano/Ta silicone) exhibited an almost identical surface chemical state regardless of the processing time. Each S-PIII treated implant had similar Ta content with stable oxide passive layers on the outermost surfaces. The heavy atomic weight of Ta combined with the application of an extremely high negative bias voltage (– 2000V) led to deep ion implantation; traces of Ta were left on the surface that subsequently combined with oxygen still present even in a vacuum [41]. Ta oxide is known to possess high chemical stability and corrosion resistance under physiological conditions, which efficiently prevented the rapid dissolution of the implanted Ta from the surface and noticeable changes to the surface topography and chemistry before and after immersion testing (**Fig. 4**) [42].

A short-term *in vitro* study was performed to investigate the cell viability of the bare and Nano/Ta silicone implants. As shown in **Fig. 7**, the bare silicone implant exhibited a low intimate cell proliferation value compared to

the Nano/Ta silicone implants. The highly hydrophobic surface of the bare silicone is generally considered to be a major factor responsible for the poor cellular response. Even though cell-recognizing proteins can adhere onto the implant surface via hydrophobic interaction, such a high surface hydrophobicity (contact angle ≈ 110°) leads to conformation changes of the adsorbed proteins and the eventual loss of their functionality [43, 44].

Based on its outstanding *in vitro* results, the Nano/Ta silicone implant was examined in a long-term *in vivo* study. Its foreign body response at the tissue–implant interface was comprehensively compared with that of the bare silicone. The Nano/Ta silicone generally exhibited substantial activity at suppressing fibrous capsule formation and contracture. As shown in **Fig. 9**, the degrees of platelet and neutrophil activation were significantly reduced around the Nano/Ta silicone implant, which is closely associated with the lower number of infiltrated macrophages around the implant (**Fig. 8**). Activated platelets and neutrophils are known to release VEGF and fibroblast growth factor that recruit macrophages [34]. Once macrophages accumulate at the tissue–implant interface, various growth factors and pro-fibrotic cytokines are secreted, which stimulate fibroblast migration and differentiation into myofibroblasts [45]. These sequential inflammatory foreign body responses lead to collagen synthesis and the eventual formation of a thick and dense fibrous capsule around the implant [6, 45].

Furthermore, among several complications associated with silicone implant, BIA-ALCL emerge as critical issues with evidence pointing at a direct association with breast implants. BIA-ALCL is a purely T-cell lymphoma that arises in either the fluid or capsule surrounding the implant, and must

be considered in any patient with implants presenting with new-onset breast swelling occurring more than a year after implantation [46]. Although the disease is limited to the periprosthetic fluid (without capsular invasion), ALCL progresses from seroma to capsular invasion, and to eventual mass formation with subsequent metastasis. Various causes associated with BIA-ALCL have been reported including textured surfaces of implants, subclinical infections, biofilms, and capsular contracture with thick capsules [47]. These eventually occur at the tissue-implant interface. The cause of BIA-ALCL is not yet clear; however, it is well known that it relates to texture-type implants. In fact, 359 cases of ALCL were reported to the FDA by 2017, of which texture-type implants accounted for the majority [48]. In cases of submuscular implants, there is no difference between the smooth and textured surface implants in the rate of capsular contracture [49]. In the present situation where BIA-ALCL has been found to be associated with textured surface implants, re-evaluation and improvements of smooth-type implants is essential. Based on this pathophysiological reason and our results, the Nano/Ta silicone implant is expected to reduce both the occurrence of BIA-ALCL as well as capsular formation by decreasing interference at the tissue-implant interface, and reduce foreign body reactions. Further studies are required on the effect of the Nano/Ta silicone implant through molecular and biological experiments on the prevention of BIA-ALCL.

V. Conclusion

This study demonstrated a new ion implantation technique for silicone implant surfaces that suppresses the foreign body response and fibrous capsule formation, which is the most common side effect of polymeric implants. S-PIII implants a high dose of biologically compatible Ta into the uppermost surface of silicone implants, which not only produces a Ta-implanted surface layer but can also generate either a smooth (Smooth/Ta silicone) or nano-textured (Nana/Ta silicone) surface morphology. Surface wettability and *in vitro* studies clearly indicated that the combination of nano-texturing and a Ta-implanted silicone surface layer (Nano/Ta silicone) was most effective at improving the hydrophilicity and fibroblast affinity compared to the bare and Smooth/Ta silicone surfaces, which demonstrates the synergistic effects of modifying both the surface topography and chemistry. In a rat *in vivo* model, factors related to fibrous capsule formation and contraction including the number of macrophages, myofibroblast differentiation and activation, and collagen density were significantly reduced around the Nano/Ta silicone implant compared to around the bare implant. These results highlight that the Ta S-PIII technique has great potential for reducing the foreign body response of implantable devices and provide important information for the design of reliable and efficient medical devices.

VI. References

1. Bachhuka A, Hayball J, Smith LE, Vasilev K. Effect of Surface Chemical Functionalities on Collagen Deposition by Primary Human Dermal Fibroblasts, ACS Appl Mater Interfaces. 2015;7(42):23767-23775.
2. Kyle DJ, Oikonomou A, Hill E, Bayat A. Development and functional evaluation of biomimetic silicone surfaces with hierarchical micro/nano-topographical features demonstrates favourable in vitro foreign body response of breast-derived fibroblasts, Biomaterials. 2015;52:88-102.
3. Magennis EP, Hook AL, Williams P, Alexander MR. Making Silicone Rubber Highly Resistant to Bacterial Attachment Using Thiol-ene Grafting, ACS Appl Mater Interfaces. 2016;8(45):30780-30787.
4. Rujitanaroj P.-o, Jao B, Yang J, Wang F, Anderson JM, Wang J, Chew SY. Controlling fibrous capsule formation through long-term down-regulation of collagen type I (COL1A1) expression by nanofiber-mediated siRNA gene silencing, Acta biomaterialia. 9(1) (2013) 4513-4524.
5. J.T. Jacob, O.J. Lacour, C.F. Burgoyne, Slow release of the antimetabolite 5-fluorouracil (5-FU) from modified Baerveldt glaucoma drains to prolong drain function, Biomaterials 2001;22(24):3329-3335.
6. Zhou G, Groth T. Host Responses to Biomaterials and Anti-Inflammatory Design-a Brief Review, Macromol Biosci. 2018;18(8):e1800112.
7. Klopfleisch R, Jung F. The pathology of the foreign body reaction against biomaterials, J Biomed Mater Res. A 2017;105(3):927-940.

8. Xu R, Luo G, Xia H, He W, Zhao J, Liu B, Tan J, et al. Novel bilayer wound dressing composed of silicone rubber with particular micropores enhanced wound re-epithelialization and contraction, Biomaterials. 2015;40:1-11.
9. Hadjesfandiari N, Yu K, Mei Y, Kizhakkedathu JY. Polymer brush-based approaches for the development of infection-resistant surfaces, Journal of Materials Chemistry B. 2014;2(31):4968-4978.
10. Vázquez González B, Meléndez Ortiz HI, Díaz Gómez L, Alvarez Lorenzo C, Concheiro A, Bucio E. Silicone rubber modified with methacrylic acid to host antiseptic drugs, Macromolecular Materials and Engineering. 2014;299(10):1240-1250.
11. Meléndez-Ortiz HI, Alvarez-Lorenzo C, Burillo G, Magariños B, Concheiro A, Bucio E. Radiation-grafting of N-vinylimidazole onto silicone rubber for antimicrobial properties, Radiation Physics and Chemistry. 2015;110:59-66.
12. Taraballi F, Sushnitha M, Tsao C, Bauza G, Liverani C, Shi A, Tasciotti E. Biomimetic Tissue Engineering: Tuning the Immune and Inflammatory Response to Implantable Biomaterials, Adv Healthc Mater. 2018;7(17):e1800490.
13. Zaveri TD, Dolgova NV, Chu BH, Lee J, Wong J, Lele TP, Ren F, et al. Contributions of surface topography and cytotoxicity to the macrophage response to zinc oxide nanorods, Biomaterials. 2010;31(11):2999-3007.
14. Mills CA, Navarro M, Engel E, Martinez E, Ginebra MP, Planell J, Errachid A, et al. Transparent micro- and nanopatterned poly(lactic acid)

for biomedical applications, J Biomed Mater Res A. 2006;76(4):781-787.

15. Zhang S, Ma B, Liu F, Duan J, Wang S, Qiu J, Li D, et al. Polylactic Acid Nanopillar Array-Driven Osteogenic Differentiation of Human Adipose-Derived Stem Cells Determined by Pillar Diameter, Nano Lett. 2018;18(4):2243-2253.
16. Lou T, Wang X, Song G, Gu Z, Yang Z. Fabrication of PLLA/beta-TCP nanocomposite scaffolds with hierarchical porosity for bone tissue engineering, Int J Biol Macromol. 2014;69:464-470.
17. Parker JA, Walboomers XF, Von den HJ, Maltha JC, Jansen JA. Soft tissue response to microtextured silicone and poly-L-lactic acid implants: fibronectin pre-coating vs. radio-frequency glow discharge treatment, Biomaterials. 2002;23(17):3545-3553.
18. Majd H, Scherer SS, Boo S, Ramondetti S, Cambridge E, Raffoul W, Friedrich M, et al. Novel micropatterns mechanically control fibrotic reactions at the surface of silicone implants, Biomaterials. 2015;54:136-47.
19. del Campo A, Arzt E. Fabrication approaches for generating complex micro- and nanopatterns on polymeric surfaces, Chem Rev. 2008;108(3):911-945.
20. Nie Z, Kumacheva E. Patterning surfaces with functional polymers, Nat Mater. 2008;7(4):277-290.
21. Pina-Hernandez C, Guo LJ, Fu PF. High-resolution functional epoxysilsesquioxane-based patterning layers for large-area nanoimprinting, ACS Nano. 2010;4(8):4776-4784.
22. Shen Y, Yao L, Li Z, Kou J, Cui Y, Bian J, Yuan C, et al. Double

transfer UV-curing nanoimprint lithography, Nanotechnology. 2013;24(46):465304.

23. Wang H, Kwok DT, Wang W, Wu Z, Tong L, Zhang Y, Chu PK. Osteoblast behavior on polytetrafluoroethylene modified by long pulse, high frequency oxygen plasma immersion ion implantation, Biomaterials. 2010;31(3):413-419.
24. Lu T, Wen J, Qian S, Cao H, Ning C, Pan X, Jiang X, et al. Enhanced osteointegration on tantalum-implanted polyetheretherketone surface with bone-like elastic modulus, Biomaterials. 2015;51:173-183.
25. Zheng C, Wang G, Chu Y, Xu Y, Qiu M, Xu M. RTV silicone rubber surface modification for cell biocompatibility by negative-ion implantation, Nuclear Instruments and Methods in Physics Research Section B: Beam Interactions with Materials and Atoms. 2016;370:73-78.
26. Zhou X, Zhang Y, Shi X, Fan D. Surface Modification of Silicone Rubber by Ion Implantation to Improve Biocompatibility, Ion Implantation-Research and Application, InTech2017.
27. Zhou X, Zhang Y, Shi X, Fan D. Preparation, Characterization, and Preliminary Biocompatibility Evaluation of Carbon Ion-Implanted Silicone Rubber, Elastomers, InTech2017.
28. Sridharan R, Cameron AR, Kelly DJ, Kearney CJ, O'Brien FJ. Biomaterial based modulation of macrophage polarization: a review and suggested design principles, Materials Today. 2015;18(6):313-325.
29. Colas A, Curtis J. Silicone biomaterials: history and chemistry, Biomaterials science: an introduction to materials in medicine. 2004;2:80-85.

30. Wang S, Shi X, Yang Z, Zhang Y, Shen L, Lei Z, Zhang Z, et al. Osteopontin (OPN) is an important protein to mediate improvements in the biocompatibility of C ion-implanted silicone rubber, PloS one. 2014;9(6):e98320.
31. Lei Z, Liu T, Li W, Shi X, Fan D. Biofunctionalization of silicone rubber with microgroove-patterned surface and carbon-ion implantation to enhance biocompatibility and reduce capsule formation, International journal of nanomedicine. 2016;11:5563.
32. Atanassova E, Dimitrova T, Koprinarova J. AES and XPS study of thin RF-sputtered Ta2O5 layers, Applied Surface Science. 1995;84(2):193-202.
33. Feng L, Zhou L, Feng S. Preparation and characterization of silicone rubber cured via catalyst-free aza-Michael reaction, RSC Advances. 2016;6(113):111648-111656.
34. Luttikhuizen DT, Harmsen MC, Van Luyn MJ. Cellular and molecular dynamics in the foreign body reaction, Tissue Eng. 2006;12(7):1955-1970.
35. Bae HS, Son HY, Lee JP, Chang H, Park JU. The Role of Periostin in Capsule Formation on Silicone Implants, Biomed Res Int 2018. 2018;3167037.
36. Levine BR, Sporer S, Poggie RA, Della Valle CJ, Jacobs JJ. Experimental and clinical performance of porous tantalum in orthopedic surgery, Biomaterials. 2006;27(27):4671-4681.
37. Balla VK, Banerjee S, Bose S, Bandyopadhyay A. Direct laser processing of a tantalum coating on titanium for bone replacement structures, Acta biomaterialia. 2010;6(6):2329-2334.

38. Gee EC, Jordan R, Hunt JA, Saithna A. Current evidence and future directions for research into the use of tantalum in soft tissue re-attachment surgery, Journal of Materials Chemistry B. 2016;4(6):1020-1034.
39. Prakash J, Pivin J, Swart H. Noble metal nanoparticles embedding into polymeric materials: from fundamentals to applications, Advances in colloid and interface science. 2015;226:187-202.
40. Jeong HC, Park HG, Lee JH, Seo DS. Localized ion-beam irradiation-induced wrinkle patterns, ACS applied materials & interfaces. 2015;7(41):23216-23222.
41. Hanawa T, Ukai H, Murakami K. X-ray photoelectron spectroscopy of calcium-ion-implanted titanium, Journal of electron spectroscopy and related phenomena. 1993;63(4):347-354.
42. Park C, Kim S, Kim HE, Jang TS. Mechanically stable tantalum coating on a nano-roughened NiTi stent for enhanced radiopacity and biocompatibility, Surface and Coatings Technology. 2016;305:139-145.
43. Nuttelman CR, Mortisen DJ, Henry SM, Anseth KS. Attachment of fibronectin to poly (vinyl alcohol) hydrogels promotes NIH3T3 cell adhesion, proliferation, and migration, Journal of Biomedical Materials Research: An Official Journal of The Society for Biomaterials, The Japanese Society for Biomaterials, and The Australian Society for Biomaterials and the Korean Society for Biomaterials. 2001;57(2):217-223.
44. Zhao D, Peng C, Zhou J, Lipase adsorption on different nanomaterials: a multi-scale simulation study, Physical Chemistry Chemical Physics.

2015;17(2):840-850.

45. Yoo BY, Kim BH, Lee JS, Shin BH, Kwon H, Koh WG, Heo CY. Dual surface modification of PDMS-based silicone implants to suppress capsular contracture. Acta Biomater 2018;76:56-70.
46. Brody GS1, Deapen D, Taylor CR, Pinter-Brown L, House-Lightner SR, Andersen JS, Carlson G, Lechner MG, Epstein AL. Analplastic large cell lymhoma occurring in women with breast implants, analysis of 173 cases. Plast Reconstr Surg. 2015;135:695-705
47. Turner SD, Inghirami G, Miranda RN, Kadin ME. Cell of origin and immunologic events in the pathogenesis of breast implant associated anaplastic large cell lymphoma. Am J Pathol. 2019; Oct 11 [Epub ahead of print]
48. K Groth A, Graf R. Breast Implant-Associated Anaplastic Large Cell Lymphoma (BIA-ALCL) and the Textured Breast Implant Crisis.Aesthetic Plast Surg. 2019 Oct 17 [Epub ahead of print]
49. Zingaretti N, Galvano F, Vittorini P, De Francesco F, Almesberger D, Riccio M, Vaienti L, Parodi PC. Smooth Prosthesis: Our Experience and Current State of Art in the Use of Smooth Sub-muscular Silicone Gel Breast Implants, Aesthetic Plast Surg. 2019;43(6):453-463

국문초록

Rat에서 탄탈륨 이온이 코팅된 실리콘 보형물의 피막형성 감소효과

이 시 우

의학과 성형외과학 전공

서울대학교 대학원

서론: 지난 수십 년 동안 생체에 적합한 폴리머 임플란트의 설계가 연구됐지만, 의도했던 폴리머 임플란트의 기능은 임플란트에 대한 숙주의 이물 반응으로 계속해서 손상되고 있다. 특히, 섬유성 캡슐의 형성 및 수축은 주변 조직과 임플란트의 치밀한 결합을 막아 임플란트의 구조 변형과 지속적인 불편함 및 통증을 초래한다. 이에 본고에서 연구자는 스퍼터링 기반 플라즈마 침지 이온 주입(S-PIII, Sputtering-based plasma immersion ion implantation)이라는 새로운 테크닉을 이용하여, 가장 널리 사용되는 폴리머 임플란트 중 하나인 실리콘 임플란트의 이물질 반응을 살펴보고자 한다.

방법: S-PIII을 이용하여 실리콘표면을 Ta 이온으로 코팅하였다. 코팅된 실리콘의 표면특징과, wettability, 그리고 물리적 특성들을 평가하였다. 순수 실리콘과 Ta이 코팅된 실리콘의 시험관내 세포 반응을 피부 섬유

아세포에 의한 세포 증식과 생존성을 통해 평가하였다. 또한, rat에서 8주간 실험을 진행하였다. 나노/Ta 실리콘 임플란트와 순수(bare)실리콘 임플란트를 rat의 등부위 근육하층에 삽입하여 생체조직-임플란트 계면에서의 이물 반응을 종합적으로 비교하고자 하였다.

결과: S-PIII는 실리콘 표면에 생물학적으로 적합한 탄탈륨(Ta)을 도입하여 탄탈륨-임플란트의 얇은층(<60 nm 두께)을 생성하여 스무스(Smooth/탄탈륨 실리콘) 또는 나노-텍스처의 (Nano/탄탈륨 실리콘) 표면 morphology을 생성해준다. Ta이온 임플란트 후 순수(bare) 실리콘의 생물학적 불활성 화학구조 및 강한 소수성 표면의 특징은 확실히 개선되었다. *in vitro* 실험결과, 세포의 증식과 생존성이 나노/Ta 실리콘 임플란트의 경우가 순수실리콘 임플란트의 경우에서 보다 증가하였음이 관찰되었다. *in vivo* 실험에서 나노/Ta 실리콘 임플란트는 섬유 캡슐 형성과 그 표면에서의 수축을 억제하였으며, 대식세포의 수, 근섬유 아세포 분화 및 활성화, 콜라겐 밀도의 분석에 근거하여 처치하지 않은 순수 실리콘 보다 더 나은 결과를 보였다.

결론: rat에서 탄탈륨 이온이 코팅된 실린콘의 피막 형성이 감소하는 효과를 확인할 수 있었다.

주요어 : 실리콘, 탄탈륨, 이온 임플란테이션, 이물질 반응

학 번 : 2014-30650